Integrated subwavelength gratings on a lithium niobate on insulator platform for mode and polarization manipulation

Xu Han
Lanzhou University
Li Chen
Lanzhou University
Yongheng Jiang
Lanzhou University
Andreas Frigg
RMIT University
Huifu Xiao
Lanzhou University
Thach Nguyen
RMIT University https://orcid.org/0000-0002-8409-5638
Andy Boes
RMIT University https://orcid.org/0000-0001-8443-3396
Jianhong Yang
Lanzhou University
Guanghui Ren
RMIT University https://orcid.org/0000-0002-9867-8279
Yikai Su
Shanghai Jiao Tong University https://orcid.org/0000-0002-1526-8187
Arnan Mitchell
RMIT University https://orcid.org/0000-0002-2463-2956
Yonghui Tian (siphoton@lzu.edu.cn)
Lanzhou University

Article

Keywords:

Posted Date: February 4th, 2022

DOI: https://doi.org/10.21203/rs.3.rs-1310958/v1

Abstract

Lithium niobate on insulator (LNOI) has emerged as a promising platform for photonic integrated circuits, with a fast-growing toolbox of components. In this paper, we propose, design and experimentally demonstrate compact subwavelength grating (SWG) waveguides on a LNOI platform for on-chip mode and polarization manipulation. To overcome the limitation of waveguide fabrication, the SWGs are designed and formed on a silicon nitride thin film deposited onto the surface of LNOI chip. As proof-of-concept devices, the SWG-based spatial mode filters and a TM-pass polarizer are fabricated successfully on the same chip, with the device lengths of only ~50 μm. The measured insertion losses for the devices are lower than 3.1 dB, with high extinction ratio larger than 30 dB, at a wavelength of 1550 nm. The proposed and demonstrated SWGs can serve as important building blocks in a series of mode and polarization handling devices for LNOI integrated photonics.

Introduction

Subwavelength gratings (SWGs), which are composed of periodically arranged dielectric segments with a pitch much smaller than the input light wavelength, have been widely investigated for developing high-performance integrated photonic devices with compact size, low loss and large bandwidth[1, 2]. In the last few years, SWG waveguides have been employed as one of the most important components to lead breakthroughs in silicon photonics, particularly for on-chip mode and polarization manipulation. A wide range of SWG-based devices including mode (de)multiplexers[3], multimode waveguide bends and crossings[4, 5], mode filters[6], polarization beam splitters[7, 8], polarizers[9], etc. have been demonstrated. The inherent advantages of the devices are driving the SWG structures to be applied on more material platforms.

Recently, lithium niobate on insulator (LNOI) has emerged as a promising platform for future photonic integrated circuits, with attractive properties such as strong modal confinement, low-loss light propagation, high-speed electro-optical modulation, and high-efficiency optical nonlinearity simultaneously[10]. With the improvements in etching of lithium niobate, the components toolbox of the LNOI platform is growing fast to satisfy the demands of varied applications, including active and passive components such as modulators[11-13], wavelength converters[14, 15], and (de)multiplexers[16-18]. As the index contrast of LNOI platform is lower than that of silicon-on-insulator (SOI) platform, the LNOI devices are suffering from relatively large footprint compared with silicon-based devices. Thus, it is attractive to form SWGs on the LNOI platform to construct compact optical components for high-density integration. However, the sidewall angle (typically 40-80°) induced by lithium niobate dry etching can limit the minimum feature size between adjacent waveguides[19], and thus, it is still not easy to fabricate SWGs with considerable controllability of the structural parameters on the LNOI platform. Moreover, the etching techniques developed for lithium niobate thin film are still specialized[20], resulting in limited duplicability compared with other platforms, e.g., SOI.

In this contribution, we propose and experimentally demonstrate compact SWG waveguide-based devices on a LNOI platform. To overcome the aforementioned challenges, a silicon nitride thin film is deposited onto the surface of the LNOI chip, where the SWGs are designed and formed using mature CMOS-compatible etching processes developed by microelectronics industry. We have noted that there are also other candidates, however, silicon nitride is one of the most promising loading materials due to its similar but slightly lower refractive index and similar transparent window to lithium niobate, as well as the mature and commercially available fabrication processes. Thus, the silicon nitride loaded LNOI waveguides can preserve the excellent material property of lithium niobate whereas overcome the challenges faced by the direct etching waveguide fabrication[21-23]. For proof-of-concept, the SWG waveguides are used to realize spatial mode filters and polarizer which are important components in mode-division multiplexing (MDM) and polarization-division multiplexing (PDM) systems, respectively. We have obtained a TE_1-mode-pass filter, a TE_2-mode-pass filter and a TM-pass polarizer with the measured insertion losses of about 1.9 dB, 3.1 dB and 1.3 dB, respectively, and the measured extinction ratio for the devices is larger than 30 dB, at a wavelength of 1550 nm. Furthermore, the fabricated device lengths are only ~50 μm. To the best of our knowledge, this is the first experimental demonstration of the compact SWG-based mode and polarization handling devices on LNOI platform.

Results

Design of SWG-based spatial mode filters. MDM has been developed for increasing the data capacity of optical interconnects by multiplexing different spatial modes in a multimode waveguide. As only a single-wavelength laser source is needed, MDM has attracted wide-spread attention due to its low cost, good system scalability and small footprint[24]. However, one of the main challenges for the MDM systems is the superposition of inter-modal crosstalk when dozens to hundreds of devices are cascaded, resulting in serious signal degradation. Mode filters are a type of devices which can filter the undesired modes out of the system, and thus help to improve the signal-to-noise ratio performance[6]. Since high-order modes have weaker confinement, they can easily be filtered out by means of tapering the waveguide to a cutoff width, hence mode filters provide usually solutions for blocking the low-order modes in a multimode waveguide[25]. Owing to the importance of the devices, several demonstrations have been reported on other material platforms[6, 25–28]. However, there are still no demonstartions for mode filters on the LNOI platform.

Figure 1a shows the schematic diagram of a proposed SWG-based TE_1-mode-pass filter. The device is designed along the crystallographic Z direction on a X-cut LNOI platform with a 300-nm-thick lithium niobate thin film on top of a 4.7-μm-thick buried oxide layer, following our previous work[23]. The birefringence of lithium niobate is considered in the design, which means the crystallographic Z direction has an extraordinary refractive index (n_e) of ~2.14, the crystallographic Y/X directions have an ordinary refractive index (n_o) of ~2.21, at a wavelength of 1550 nm. The SWG structure is designed on a silicon nitride thin film on the surface of the LNOI platform, whose thickness is chosen to be 300 nm as well, for a strong mode confinement in the hybrid waveguide and a considerable mode confinement factor in the

lithium niobate slab[29]. As silicon nitride has similar but slightly lower refractive index to lithium niobate (~1.99), the input optical mode is partially confined in the silicon nitride rib, which is important for the interaction between the optical mode and SWG structure.

For a TE_1-mode-pass filter, the hybrid SWG waveguide is expected to work in the Bragg regime for TE_0 mode and the subwavelength regime for TE_1 mode. Thus, the input TE_0 mode is reflected whereas the TE_1 mode is converted to the localized Bloch mode and propagates with low loss. It means that the Bragg conditions should be satisfied, which are expressed as[30]:

$$\Lambda_1 = \lambda_0 / \left(2 \cdot n_{eff0}\right) < \lambda_0 / \left(2 \cdot n_{eff1}\right) \quad (1)$$

where Λ_1 is the grating pitch, λ_0 is the central wavelength of photonic stop band for TE_0 mode, n_{eff0} and n_{eff1} are the effective indices of TE_0 and TE_1 modes in the hybrid SWG waveguide.

The SWG structure is optically equivalent to a homogeneous medium with a refractive index given by[1]:

$$n_{SWG}^2 = n_{SiN}^2 \cdot ff + n_{air}^2 \cdot (1 - ff)$$

2

where n_{SiN} and n_{air} are the refractive indices of silicon nitride and air clad, respectively. The *ff* is the filling factor of the SWG, which is expressed as $ff = w_t/\Lambda_1$ where w_t is the width of the SWG segment. Here, the *ff* is designed to be 0.7, for an easy-to-fabricate minimum feature size as well as a relatively large effective index difference between different modes. Then, the effective refractive indices of the Bloch modes in the hybrid SWG waveguide are calculated by using a full-vector eigenmode solver[31], as shown in Figure 1b. According to the results, the width of the SWG is designed to be w_1=2 μm for low-loss propagation of TE_1 mode, and the grating pitch is designed to be Λ_1 = 413 nm for a photonic stopband of TE_0 mode around 1550 nm. The transmission of TE_0 and TE_1 modes as a function of grating period number is simulated at a wavelength of 1550 nm, by using the three-dimensional finite-difference time domain (3D-FDTD) method[32], as shown in Figure 1c. To achieve both low loss and high mode extinction ratio (MER), the grating period number is chosen to be 120. The simulated insertion loss for TE_1 mode is 1.7 dB and the MER between TE_0 and TE_1 modes is about 48 dB. The total length of our SWG-based TE_1-mode-pass filter is 49.56 μm. Figure 1d shows the simulated electric field profiles for TE_0 and TE_1 modes input into the device, at a wavelength of 1550 nm. It can be seen that the TE_1 mode passes through the device with low loss whereas the TE_0 mode is blocked. We also simulate the transmission spectra of different modes as a function of the input wavelength, as shown in Figure 1e. The designed device shows a bandwidth of about 46 nm (from 1524 nm to 1570 nm) for a MER larger than 20 dB, while the insertion loss for TE_1 mode stays below 3.5 dB.

Most of the demonstrated mode filters block only one specific low-order mode, generally TE_0 mode. It is still difficult to deal with the case that multiple modes need to be filtered out simultaneously, however, this function is important for the real-world application of the devices. Researchers proposed a few methods to solve this problem, such as cascading multiple directional couplers[26], or introducing graphene as auxiliary material[27], however, such devices have typically large footprint and relatively low extinction ratio. Thus, a compact and high-extinction-ratio mode filter which can filter out multiple optical modes simultaneously is still missing as a photonic circuit component. To fill this gap, we demonstrate our SWGs as an attractive choice to realize such a mode filter on the LNOI platform. For proof-of-concept, a TE_2-mode-pass filter is designed here.

Figure 2a shows the schematic diagram of the proposed TE_2-mode-pass filter. The hybrid SWG waveguide is designed to work in the subwavelength regime for TE_2 mode, while work in the Bragg regime for TE_0 and TE_1 modes simultaneously. The Bragg conditions have been revised as:

$$\lambda_1/\left(2\cdot n_{eff0}\right)<\Lambda_2<\lambda_1/\left(2\cdot n_{eff1}\right)<\lambda_1/\left(2\cdot n_{eff2}\right) \qquad (3)$$

where Λ_2 is the grating pitch, λ_1 is the working wavelength, n_{eff0}, n_{eff1} and n_{eff2} are the effective indices of TE_0, TE_1 and TE_2 modes in the hybrid SWG waveguide. For simplicity, we also design the *ff* to be 0.7, while the width of SWG is chosen to be w_2= 3.5 μm to support low-loss propagation of TE_2 mode, as shown in Figure 2b. It can also be seen that the effective index difference between TE_0 and TE_1 modes is smaller than that between TE_1 and TE_2 modes. Thus, it can be predicted that the photonic stopbands of TE_0 and TE_1 modes are located closely to each other whereas well separated from that of TE_2 mode, which is important for filtering out the TE_0 and TE_1 modes simultaneously. According to the results, the grating pitch is designed to be Λ = 415 nm for a device working at around 1550 nm. We also simulated the power transmission for different modes as a function of the grating period number at a wavelength of 1550 nm, by using 3D-FDTD method again, as shown in Figure 2c. According to the results, the grating period number is chosen to be 120 as well, resulting in the total length of the device to be 49.8 μm. The insertion loss for TE_2 mode is 1.2 dB and the MER between TE_2 and the low-order modes is larger than 41 dB. Figure 2d shows the simulated electric field profiles for TE_0, TE_1 and TE_2 modes input into the device, at a wavelength of 1550 nm. It can be seen that TE_2 mode passes through the device with low loss whereas the low-order modes are blocked. Similarly, Figure 2e shows the transmission spectra of different modes as a function of the input wavelength. The designed device shows a bandwidth of 33 nm (from 1533nm to 1566 nm) for a MER larger than 20 dB, while the insertion loss for TE_2 mode stays below 4.2 dB.

Design of SWG-based TM-pass polarizer. Similar to spatial mode filters, polarizer can stop one of the two polarization modes while let the other one pass, and it plays a key role in PDM systems to reduce the

crosstalk. Due to its attractive function, TE/TM-pass polarizers have been widely investigated based on different structures on the SOI platform[9, 33–35]. Fortunately, there are also a few works reported previously on the LNOI platform. For example, hybrid plasmonic gratings (HPG) have been proposed and numerically demonstrated for TE/TM-pass polarizers on the LNOI platform[36, 37]. The proposed devices are compact with only several to tens of micros length, and broadband with high polarization extinction ratio (PER). However, the metal deposition requires high alignment accuracy, which is not easy in the real-world fabrication. Furthermore, the devices will suffer high additional absorption loss from the metal. On the other hand, lateral leakage has also been proposed to realize TE/TM-pass polarizers by differentiating the propagation loss of TE and TM modes in a waveguide[38, 39]. This kind of device is expected to have low loss and high PER. However, the devices are usually required to be from hundreds of micros to one millimeter long, which are somewhat bulky for large-scale integration. Thus, there is still a gap to realize a polarizer with compact size, low loss and high PER simultaneously based on the LNOI platform. To address this gap, we demonstrate a compact, low-loss and high-PER TM-pass polarizer by using our SWGs.

Figure 3a shows the schematic diagram of the proposed SWG-based TM-pass polarizer which is designed along the crystallographic Y direction on the same platform as the mode filters. The width of the silicon nitride stripe is set to be w_3=1 μm, which can support low loss propagation for both TE_0 and TM_0 modes while the high-order modes are cut-off in the hybrid waveguide. For a TM-pass polarizer, the SWG waveguide is expected to work in the Bragg regime for TE_0 mode while work in the subwavelength regime for TM_0 mode. It means that the Bragg conditions should be expressed as:

$$\Lambda_3=\lambda_0/\left(2\cdot n_{effTE}\right)<\lambda_0/\left(2\cdot n_{effTM}\right) \qquad (4)$$

where λ_0 is the central wavelength of photonic stopband for TE_0 mode, n_{effTE} and n_{effTM} are the effective indices of TE_0 and TM_0 modes in the hybrid SWG waveguide. To avoid the mode hybridization in the Y propagating waveguide, the *ff* is chosen to be 0.8 and a nanobridge with a width of w_4= 100 nm is designed to connect the segments (refer to Supporting Information, S1 for details).

Figure 3b shows the calculated effective indices of Bloch modes in the hybrid SWG waveguide. It can be seen that the TM_0 mode is cutoff when the SWG width is below 1.75 μm. Thus, the width of the SWG is chosen to be w_5=1.8 μm for low loss propagation of TM_0 mode, as well as a large effective index difference between TE_0 and TM_0 modes. According to the results, the grating pitch is chosen to be Λ_3 = 422 nm in this work, for a central wavelength around 1550 nm. Figure 3c shows the simulated transmission of TE_0 and TM_0 modes as a function of grating period number is simulated at a wavelength of 1550 nm. The input and output modes are designed to converted to and from the Bloch modes gradually by means of SWG tapers, for reducing mode conversion loss. According to the simulated

results, the number of grating periods is chosen to be 110 for both low loss and high PER. It can be seen that the simulated insertion loss for TM_0 mode is about 0.5 dB, and the PER is about 38 dB. The SWGs are designed to connect with the silicon nitride stripes by using a pair of tapers with a length of L_t=4.5 μm. The total length of the device is ~55 μm, with the length of taper waveguides included, which is reduced greatly compared to that reported in previous work on the same platform (~1000 μm)[38]. Figure 3d shows the simulated electric field profiles for TE_0 and TM_0 modes input into the device, at a wavelength of 1550 nm. Figure 3e shows the simulated transmission spectra of different light polarization modes as a function of the input wavelength. It can be seen that the designed device shows a bandwidth of about 39 nm (from 1526-1565 nm) for a 20 dB PER, and the insertion loss for TM_0 mode is below 0.6 dB within this wavelength range.

Device characteristics. Figure 4a shows the microscope image of the fabricated devices for TE_1-mode-pass filter, with a close-up scanning electron microscope (SEM) image of the SWGs. For the convenience of measurement, TE_0-TE_1 mode (de)multiplexers (MMUXs) are fabricated and connected to the TE_1-mode-pass filter[23]. The input and output ports for TE_0 mode are denoted as I_0-O_0, while those for TE_1 mode are denoted as I_1-O_1, respectively. In order to eliminate the effects from the MMUXs to the device performance, a reference device with the SWGs replaced by silicon nitride stripe is fabricated closely on the same chip (refer to Supporting Information, S2 for details). The corresponding ports are denoted as I_2-O_2 and I_3-O_3 for TE_0 and TE_1 modes, respectively. Figure 4b shows the microscope image of the fabricated devices for TE_2-mode-pass filter, with the SWGs shown in a SEM image as well. Similarly, TE_0-TE_1-TE_2 MMUXs are fabricated and connected to the filter for the convenience of multimode input and output[23]. The input and output ports are denoted as I_0-O_0, I_1-O_1 and I_2-O_2 for TE_0, TE_1 and TE_2 modes, respectively. The experimental results are also normalized to that of the reference device without SWGs (refer to Supporting Information, S3 for details). The devices are interfaced by grating couplers with a grating period of 920 nm and duty circle of 0.4. The details of grating couplers can be found in our previous work[40].

Figure 4c shows the measured results of the TE_1-mode-pass filter which are normalized to the reference device without SWGs. At a wavelength of 1550 nm, the device show insertion loss for TE_1 mode of 1.9 dB and a MER of about 43 dB. Moreover, the experimental results exhibit a bandwidth of ~44 nm (from 1515-1559 nm) for a MER of 20 dB, and the insertion loss for TE_1 mode is lower than 3.2 dB within the wavelength range. Figure 4d shows the measured results of the TE_2-mode-pass filter. The measured insertion loss for TE_2 mode is 3.1 dB, and the MER is about 34 dB, at a wavelength of 1550 nm. Moreover, the device shows a bandwidth of ~29 nm (from 1525-1554 nm) for a MER of 20 dB, and the insertion loss for TE_2 mode is lower than 6 dB within this wavelength range.

Figure 5a shows the microscope image of the fabricated devices for TM-pass polarizer, including the SEM image of the SWGs with a nanobridge. We use the polarization splitter and rotator (PSR) to input and output different polarization modes for the ease of measurement[23]. The input and output ports for

TE_0 mode are denoted as I_0 and O_0, while those for TM_0 mode are denoted as I_1 and O_1, respectively. The reference device without the SWGs is also fabricated (refer to Supporting Information, S4 for details). The devices are interfaced by grating couplers with a grating period of 940 nm and duty circle of 0.4[40]. The normalized results are shown in Figure 5b. The measured insertion loss for TM_0 mode is about 1.3 dB, and the PER is about 30.6 dB, at a wavelength of 1550 nm. The fabricated device shows a bandwidth of ~36 nm (from 1521-1557 nm) for a PER of 20 dB, and the insertion loss for TM_0 mode is lower than 1.5 dB within the 36 nm wavelength range.

Overall, the measured results are close to our simulation. We have noted the measured central wavelengths of the photonic stopbands are blue shifted compared with the design. This can be attributed to the slight deviations in the fabrication. Even so, the fabricated devices still provide good performance in the C band. The central wavelengths can be tuned to desired wavelengths by a precompensation of the structural parameters in the future.

Discussion

To the best of our knowledge, this is the first demonstration of higher-order mode pass filter on the LNOI platform. Our mode filter provides an attractive choice due to its compact size, low loss, high MER and scalable functionality, even compared with the devices reported on other material platforms (refer to Supporting Information, S5 for details). Moreover, our device can also be fabricated by using mature CMOS-compatible etching processes developed by microelectronics industry, while preserve the ability to explore high-speed electro-optic devices and high-efficiency optical nonlinear devices based on the LNOI platform.

A brief summary of previously reported TM-pass polarizers on the LNOI platforms is provided in **Table. 1**. So far, there are still few experimental demonstrations of TM-pass polarizer on the LNOI platforms. It can be seen that the demonstrated device provides one of the best options to have compact size, low loss and high PER simultaneously.

In summary, we have investigated SWG waveguides for on-chip mode and polarization manipulation on a silicon nitride loaded LNOI platform. The proposed SWGs are compact and easy-to-fabricate, benefiting from the maturely developed fabrication processes of silicon nitride. In support of this, the SWG-based spatial mode filters and TM-pass polarizer are designed and fabricated successfully, with the device lengths of ~50 μm. For spatial mode filters, we have obtained a TE_1-mode-pass filter and a TE_2-mode-pass filter for blocking the low-order modes in a multimode waveguide. The measured insertion losses for TE_1 and TE_2 modes are 1.9 dB and 3.1 dB, respectively, and the MER is larger than 34 dB, at a wavelength of 1550 nm. For a TM-pass polarizer, the measured insertion loss for TM_0 mode is 1.3 dB, and the PER is 30.6 dB, at a wavelength of 1550 nm. Moreover, the fabricated devices show reasonable wide bandwidths for a high ER larger than 20 dB, which can also be used for further applications combining the MDM/PDM with the wavelength-division multiplexing (WDM) technology. The demonstrated SWGs are

expected to be implemented into a large number of compact optical components for mode and polarization manipulation on the LNOI platform.

Table 1
Comparison of some TM-pass polarizers reported on LNOI platforms

Reference	Results	Size (μm)	Loss at 1550 nm (dB)	PER at 1550 nm (dB)
[36]	Simulated	23	~2	~20
[38]	Simulated	1000	~0.3	~24
[39]	Experimental	300	~2	~20
This work	Experimental	55	1.3	30.6

Methods

Device fabrication. We fabricated the devices on a LNOI chip provided by NanoLN, with the designed parameters. The silicon nitride thin film is deposited onto the surface of the LNOI chip by using reactive sputtering, following our previous work[41]. The waveguide and grating coupler structures are formed by a single-step electron beam lithography (EBL) following by inductively coupled plasma etching process.

Device characterization. We measured the fabricated devices by using a tunable laser, a polarization controller, an off-chip circulator, and an optical spectrum analyzer. In the experiment, light with a wavelength range of 1500-1580 nm is transmitted from the tunable laser to the polarization controller, then passes through the circulator and on-chip devices, finally is received by the optical spectrum analyzer (refer to Supporting Information, S6 for details). The off-chip circulator aims to prevent the high-power reflected light from damaging the tunable laser.

Data Availability

The data that support the findings of this study are available from the corresponding author upon reasonable request.

Declarations

Acknowledgements

This work was supported by National Key R&D Program of China (2021YFB2800100), National Natural Science Foundation of China (NSFC) (62075091), Fundamental Research Funds for the Central Universities (lzujbky-2021-pd11), and Australian Research Council (ARC) grants (DP190102773). The authors acknowledge the facilities, and the scientific and technical assistance, of the Micro Nano Research Facility (MNRF) and the Australian Microscopy & Microanalysis Research Facility at RMIT

University. This work was performed in part at the Melbourne Centre for Nanofabrication (MCN) in the Victorian Node of the Australian National Fabrication Facility (ANFF).

Author contributions

X.H. and L.C. conceived and performed the device design. A.F. and G.R. carried out the device fabrication. X.H., Y.J. and H.X. carried out the device characterization. X.H. and Y.T. carried out the data analysis. X.H. wrote the paper with the assistance of Y.T., T.G.N., A.B., J.Y., Y.S. and A.M.. G.R. and Y.T. supervised this project.

Competing interests

The authors declare no competing interests.

Additional information

Supplementary information is available for this paper at xxx.

Correspondence and requests for materials should be addressed to G.R. or Y.T.

References

1. Cheben, P., Halir, R., Schmid, J. H., Atwater, H. A. & Smith, D. R. Subwavelength integrated photonics. Nature **560**, 565–572 (2018).
2. Luque-González, J. M. et al. A review of silicon subwavelength gratings: building break-through devices with anisotropic metamaterials. Nanophotonics **10**, 2765–2797 (2021).
3. He, Y. et al. Silicon high-order mode (de) multiplexer on single polarization. J. Lightwave Technol. **36**, 5746–5753 (2018).
4. Wu, H. et al. Ultra-sharp multimode waveguide bends with subwavelength gratings. Laser Photonics Rev. **13**, 1800119 (2019).
5. Wu, S. et al. A compact and polarization-insensitive silicon waveguide crossing based on subwavelength grating MMI couplers. Opt. Express **28**, 27268–27276 (2020).
6. Guan, X., Ding, Y. & Frandsen, L. H. Ultra-compact broadband higher order-mode pass filter fabricated in a silicon waveguide for multimode photonics. Opt. Lett. **40**, 3893–3896 (2015).
7. Li, C., Zhang, M., Bowers, J. E. & Dai, D. Ultra-broadband polarization beam splitter with silicon subwavelength-grating waveguides. Opt. Lett. **45**, 2259–2262 (2020).
8. Luque-González, J. M. et al. Polarization splitting directional coupler using tilted subwavelength gratings. Opt. Lett. **45**, 3398–3401 (2020).
9. Guan, X. et al. Low-loss ultracompact transverse-magnetic-pass polarizer with a silicon subwavelength grating waveguide. Opt. Lett. **39**, 4514–4517 (2014).

10. Boes, A., Corcoran, B., Chang, L., Bowers, J. & Mitchell, A. Status and potential of lithium niobate on insulator (LNOI) for photonic integrated circuits. Laser Photonics Rev. **12**, 1700256 (2018).
11. Wang, C. et al. Integrated lithium niobate electro-optic modulators operating at CMOS-compatible voltages. Nature **562**, 101–104 (2018).
12. He, M. et al. High-performance hybrid silicon and lithium niobate Mach–Zehnder modulators for 100 $Gbits^{-1}$ and beyond. Nat. Photonics **13**, 359–364 (2019).
13. Xu, M. et al. Dual-polarization thin-film lithium niobate in-phase quadrature modulators for terabit-per-second transmission. Optica **9**, 61–62 (2022).
14. Yuan, S. et al. Strongly enhanced second harmonic generation in a thin film lithium niobate heterostructure cavity. Phys. Rev. Lett. **127**, 153901 (2021).
15. Wang, L., Zhang, X. & Chen, F. Efficient second harmonic generation in a reverse-polarization dual-layer crystalline thin film nanophotonic waveguide. Laser Photonics Rev., 2100409 (2021).
16. Zhang, M., Chen, K., Wang, M., Wu, J. & Chiang, K. S. Electro-optic reconfigurable two-mode (de) multiplexer on thin-film lithium niobate. Opt. Lett. **46**, 1001–1004 (2021).
17. Chen, Z., Yang, J., Wong, W.-H., Pun, E. Y.-B. & Wang, C. Broadband adiabatic polarization rotator-splitter based on a lithium niobate on insulator platform. Photonics Res. **9**, 2319–2324 (2021).
18. Chen, G. et al. Four-channel CWDM device on a thin-film lithium niobate platform using an angled multimode interferometer structure. Photonics Res. **10**, 8–13 (2022).
19. Zhu, D. et al. Integrated photonics on thin-film lithium niobate. Adv. Opt. Photonics **13**, 242–352 (2021).
20. Yang, S. et al. Highly-efficient thin film $LiNbO_3$ surface couplers connected by ridge-waveguide subwavelength gratings. J. Mater. Sci: Mater. Electron. (2021).
21. Ahmed, A. N. R. et al. High-efficiency lithium niobate modulator for K band operation. APL Photonics **5**, 091302 (2020).
22. Chang, L. et al. Thin film wavelength converters for photonic integrated circuits. Optica **3**, 531–535 (2016).
23. Han, X. et al. Mode and polarization-division multiplexing based on silicon nitride loaded lithium niobate on insulator platform. Laser Photonics Rev. **16**, 2100529 (2022).
24. Li, C., Liu, D. & Dai, D. Multimode silicon photonics. Nanophotonics **8**, 227–247 (2018).
25. Ahmmed, K. T., Chan, H. P. & Li, B. Broadband high-order mode pass filter based on mode conversion. Opt. Lett. **42**, 3686–3689 (2017).
26. Ahmmed, K. T., Chan, H. P. & Li, B. Scalable selective high order mode pass filter architecture with asymmetric directional couplers. Opt. Express **28**, 28465–28478 (2020).
27. Xing, Z. et al. Waveguide-integrated graphene spatial mode filters for on-chip mode-division multiplexing. Opt. Express **27**, 19188–19195 (2019).
28. Sun, C., Wu, W., Yu, Y., Zhang, X. & Reed, G. T. Integrated tunable mode filter for a mode-division multiplexing system. Opt. Lett. **43**, 3658–3661 (2018).

29. Boes, A. et al. Improved second harmonic performance in periodically poled LNOI waveguides through engineering of lateral leakage. Opt. Express **27**, 23919–23928 (2019).
30. Halir, R. et al. Waveguide sub-wavelength structures: a review of principles and applications. Laser Photonics Rev. **9**, 25–49 (2015).
31. Nguyen, T. G., Tummidi, R. S., Koch, T. L. & Mitchell, A. Rigorous modeling of lateral leakage loss in SOI thin-ridge waveguides and couplers. IEEE Photonics Technol. Lett. **21**, 486–488 (2009).
32. Snyder, A. W. & Love, J. D. Modal methods for Maxwell's equations. *Optical Waveguide Theory* (Springer, New York, 1983).
33. Liu, W., Dai, D. & Shi, Y. High-performance all-silicon polarizer with 415 nm bandwidth. Opt. Lett. **46**, 1321–1324 (2021).
34. He, Y., Zhang, Y., Zhang, R., Sun, L. & Su, Y. Ultra-compact and broadband silicon polarizer employing a nanohole array structure. Opt. Lett. **46**, 194–197 (2021).
35. Chen, R., Bai, B. & Zhou, Z. Low-loss hybrid plasmonic TM-pass polarizer using polarization-dependent mode conversion. Photonics Res. **8**, 1197–1202 (2020).
36. Yu, W., Dai, S., Zhao, Q., Li, J. & Liu, J. Wideband and compact TM-pass polarizer based on hybrid plasmonic grating in LNOI. Opt. Express **27**, 34857–34863 (2019).
37. Dai, S. et al. Broadband and Compact TE-Pass Polarizer Based on Hybrid Plasmonic Grating on LNOI Platform. IEEE Photonics J. **13**, 1–9 (2020).
38. Liu, Y. et al. TE/TM-pass polarizers based on lateral leakage in a thin film lithium niobate–silicon nitride hybrid platform. Opt. Lett. **45**, 4915–4918 (2020).
39. Jin, W. & Chiang, K. S. Leaky-mode long-period grating on a lithium-niobate-on-insulator waveguide. Optica **8**, 1624–1631 (2021).
40. Han, X. et al. Single-step etched grating couplers for silicon nitride loaded lithium niobate on insulator platform. APL Photonics **6**, 086108 (2021).
41. Frigg, A. Low loss CMOS-compatible silicon nitride photonics utilizing reactive sputtered thin films. Opt. Express **27**, 37795–37805 (2019).

Figures

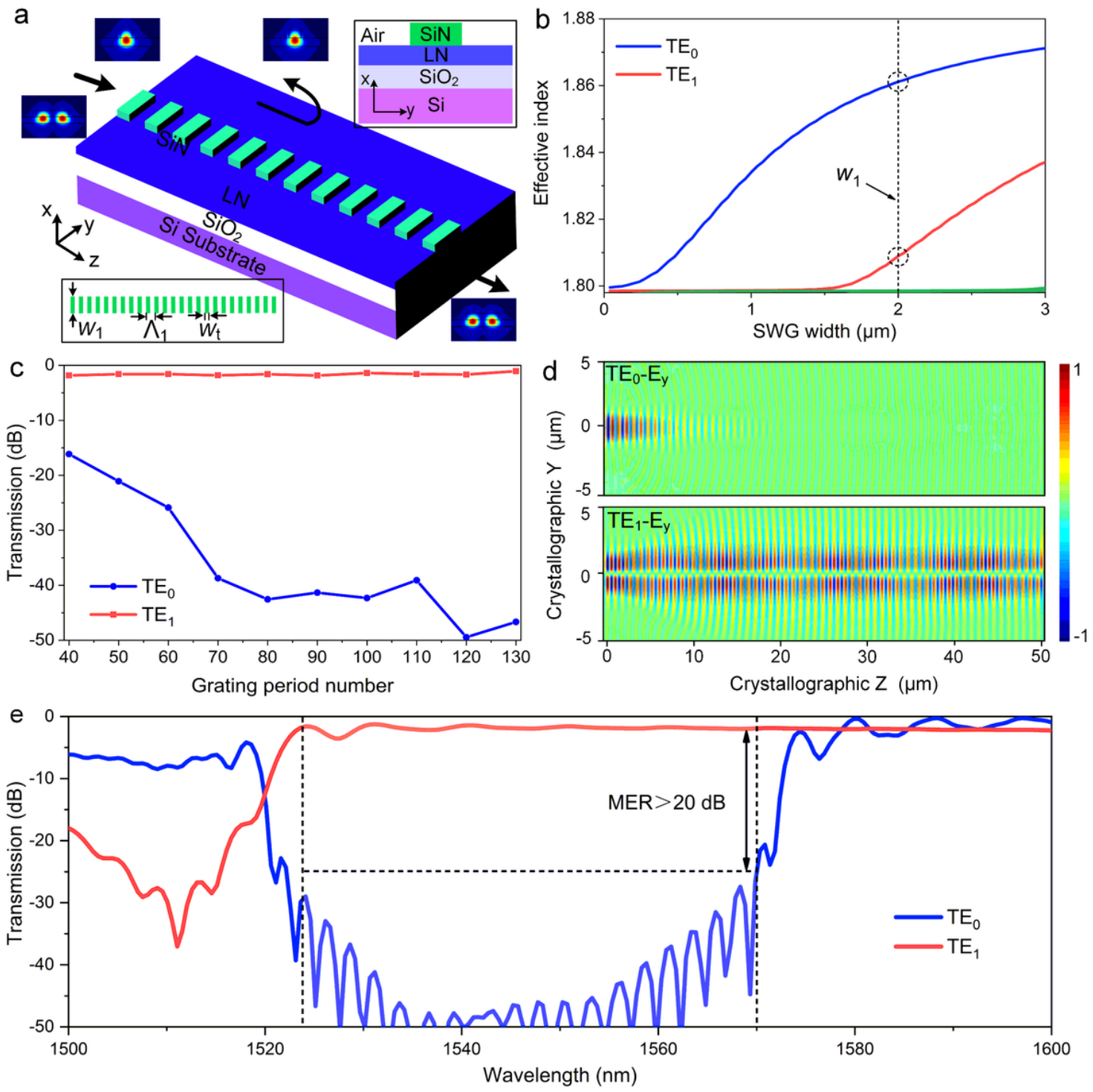

Figure 1

Design of TE_1-mode-pass filter. a Schematic diagram of the proposed TE_1-mode-pass filter. **b** Calculated mode effective indices as a function of SWG width in the Z-propagating hybrid SWG waveguide with a *ff* of 0.7. **c** Simulated transmission of TE_0 and TE_1 modes as a function of grating period number. **d** Simulated electric field profiles for TE_0 and TE_1 modes input into the device, at a wavelength of 1550 nm. **e** Simulated transmission spectra of different modes as a function of the input wavelength.

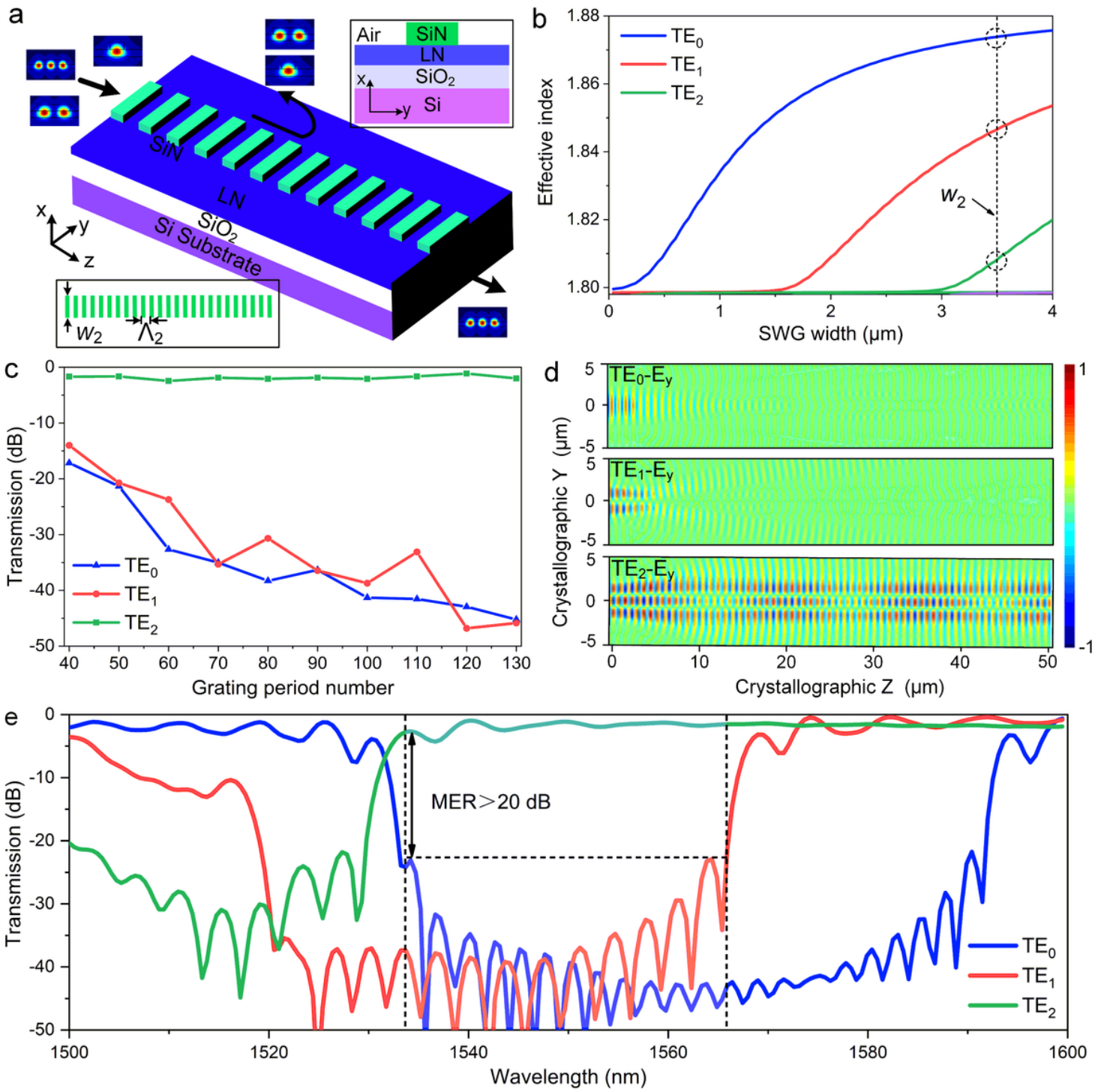

Figure 2

Design of TE_2-mode-pass filter. a Schematic diagram of the proposed TE_2-mode-pass filter, **b** Calculated mode effective indices as a function of SWG width in the Z-propagating hybrid SWG waveguide with a *ff* of 0.7, **c** Simulated transmission of TE_0, TE_1 and TE_2 modes as a function of grating period number, **d** Simulated electric field profiles for TE_0, TE_1 and TE_2 modes input into the device, at a wavelength of 1550 nm, **e** Simulated transmission spectra of different modes as a function of the input wavelength.

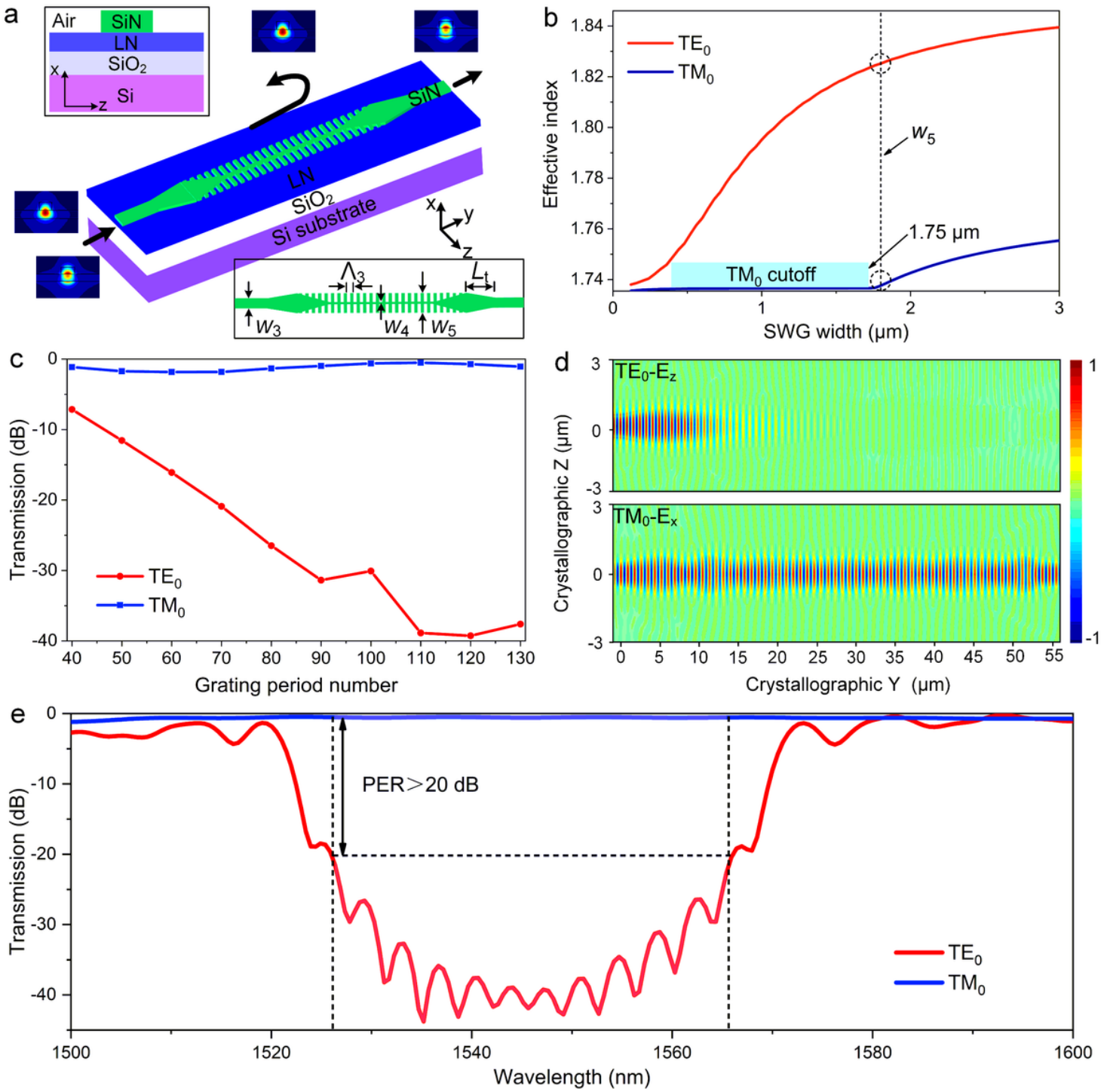

Figure 3

Design of TM-pass polarizer. a Schematic diagram of the proposed TM-pass polarizer. **b** Calculated mode effective indices as a function of SWG width in the Y-propagating hybrid SWG waveguide with a 100-nm-wide nanobridge and the *ff* is 0.8. **c** Simulated transmission of TE_0 and TM_0 modes as a function of grating period number. **d** Simulated electric field profiles for TE_0 and TM_0 modes input into the device, at a wavelength of 1550 nm. **e** Simulated transmission spectra of different polarization modes as a function of the input wavelength.

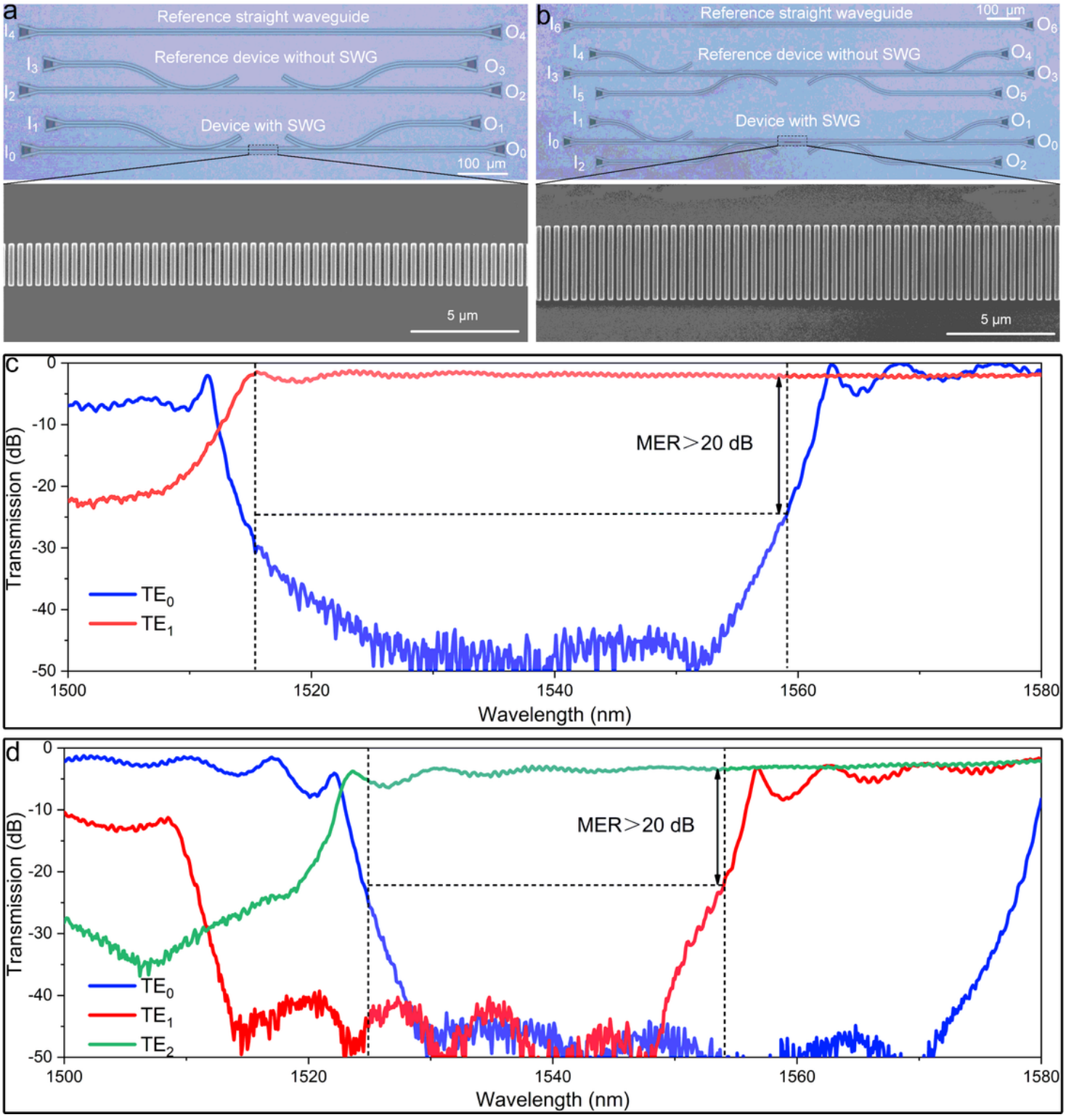

Figure 4

Experimental demonstration for spatial mode filters. a Microscope image of the fabricated devices for TE_1-mode-pass filter, with a close-up SEM image of the SWGs. **b** Microscope image of the fabricated devices for TE_2-mode-pass filter, with a close-up SEM image of the SWGs. **c** Experimental results of TE_1-mode-pass filter. **d** Experimental results of TE_2-mode-pass filter.

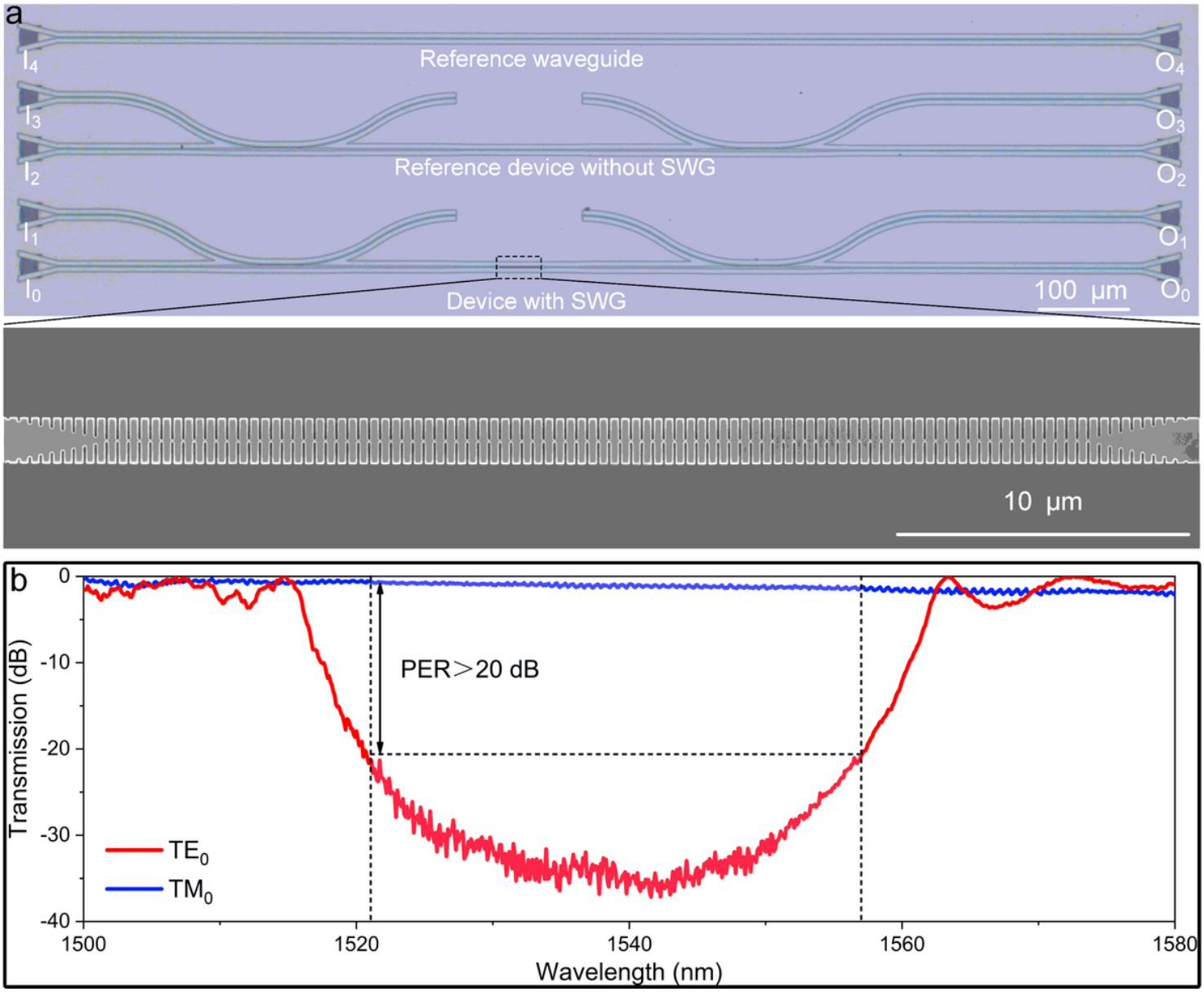

Figure 5

Experimental demonstration for TM-pass polarizer. a Microscope image of the fabricated devices for TM-pass polarizer, with a close-up SEM image of the SWGs. **b** Experimental results of the TM-pass polarizer.

Supplementary Files

This is a list of supplementary files associated with this preprint. Click to download.

- SupplementaryInformation.docx